The Effect of Field-Dependent n-Value on Screening Current, Voltage, and Magnetic Field of REBCO Coil

Jeseok Bang, Kwangmin Kim, Griffin Bradford, Jonathan Lee, Dmytro Abraimov, *Member, IEEE*, Takanobu Mato, So Noguchi, *Member, IEEE*, Seungyong Hahn, and David Larbalestier, *Life Fellow, IEEE*

***Abstract*—Here we report the effect of field-dependent index value $n(B,\theta)$ on screening current and consequential NI REBCO coil behavior. Through the 'Little Big Coil (LBC)' framework, an unexpected voltage behavior has been observed at the top and bottom coils in the fourth mini magnet LBC4 during the self-field operation at 77 K. The measurement demonstrates that the top/bottom coil voltage is temporarily decreased and then increased. However, this anomaly cannot be reproduced if the conventional simulation model uses the power-law $E-J$ model with a constant n-value. Hence, we have revisited a property of the REBCO-coated conductor and, as a result, found that the field dependency of n is necessary to elucidate the behavior. This paper will provide the 77 K self-field operation results, e.g., module coil voltages and the central magnetic field. A numerical simulation considering the field dependency investigates unexpected coil voltage behavior. The comparison between simulation results if the dependency is included and if not will be discussed.**

***Index Terms*—Coil modeling, field dependency, magnetic field hysteresis, REBCO-coated conductor, screening current.**

I. Introduction

SCREENING current of REBCO-coated conductor causes excessive magnetic stress, thus probably constraining the design versatility of high-field REBCO magnet. Hence, researchers have made numerous research and development endeavors regarding practical technologies to break through the magnet design issue. For this, the numerical simulation of screening current-induced stress (SCS) on REBCO applications has been widely used, and indeed, the results have offered intriguing ideas and reasonable conclusions [1], [2], [3], [4], [5], [6], [7], [8], [9].

Manuscript received 25 September 2023; revised 13 December 2023; accepted 15 January 2024. Date of publication 23 January 2024; date of current version 6 February 2024. This work was supported in part by the National Science Foundation Cooperative performed at National High Magnetic Field Laboratory, under Agreement DMR-2128556, in part by the State of Florida, and in part by the DOE Office of Fusion Energy Sciences under Grant DE-SC0022011. *(Corresponding author: Jeseok Bang.)*

Jeseok Bang, Kwangmin Kim, Griffin Bradford, Jonathan Lee, Dmytro Abraimov, and David Larbalestier are with the National High Magnetic Field Laboratory, Florida State University, Tallahassee, FL 32310 USA (e-mail: jbang@asc.magnet.fsu.edu).

Takanobu Mato and So Noguchi are with the Graduate School of Information Science and Technology, Hokkaido University, Sapporo 060-0814, Japan.

Seungyong Hahn is with the Department of Electrical and Computer Engineering, Seoul National University, Seoul 08826, South Korea.

Color versions of one or more figures in this article are available at https://doi.org/10.1109/TASC.2024.3357472.

Digital Object Identifier 10.1109/TASC.2024.3357472

The power-law $E-J$ model of REBCO-coated conductor (CC) [10] is essential in the screening current simulation [11], [12], [13], [14], [15], [16]. The law is derived from the $I-V$ curve, the current and voltage measurement results, where the key parameters are critical current I_c and index value n. They depend on fields and temperatures, thus investigated in various field environments, e.g., field intensity B and angle θ [17], [18], [19]. Accordingly, the recent simulations consider the field-dependent critical current $I_c(B,\theta)$. However, few simulations have considered $n(B,\theta)$, so the effect has been insufficiently discussed [20], [21].

Through the 'Little Big Coil (LBC)' framework [22], [23], we have recently confirmed that the use of a constant n-value may be deficient in the screening current analysis. Last late March, the fourth mini magnet LBC4, a stack of twelve no-insulation (NI) REBCO coils, operated in self-field at 77 K, self-field at 4.2 K, and 31.1 T in-field at 4.2 K. An unexpected voltage behavior at the top and bottom coils was observed in the self-field operation at 77 K. The measurement demonstrates that the top/bottom module coil voltage is temporarily decreased and then increased, which cannot be reproduced by the conventional simulations [24] if the power-law $E-J$ model with a constant n-value is used. Hence, we have revisited a property of the REBCO-coated conductor and, as a result, confirmed that the field-dependent index value $n(B,\theta)$ is necessary to elucidate the behavior.

This paper provides the 77 K self-field operation results, e.g., module coil voltages and hysteresis of the central magnetic field. A numerical simulation considering the field dependency investigates unexpected coil voltage behavior. The comparison between simulation results is discussed if the dependency is included and if not. Finally, we conclude that $n(B,\theta)$ should be considered in the numerical simulation for estimating screening current induction to a reasonable extent.

II. Materials and Methods

Table I shows the key parameters used for this work. SuperPower AP tape is used for the fabrication. LBC4 almost replicates the geometry specifications of its antecedent mini magnet LBC3 that was used to explore the record-high 45.5 T with 31.1 T Bitter-plate resistive background magnet [22].

Fig. 1 presents measured $I_c(B,\theta)$ and $n(B,\theta)$ at 77 K. From the in-field measurement results, the correlation between $I_c(B,\theta)$ and $n(B,\theta)$ is obtained by a linear regression approach

TABLE I
KEY PARAMETERS OF A SOLENOID MAGNET

Conductor parameters	Unit	
Manufacturer		SuperPower
Conductor width	[mm]	4.0
Conductor thickness	[μm]	45
Magnet parameters		
Number of single pancake		12
Number of turns per pancake		220
Inner and outer diameter	[mm]	14.0;34.0
Total height	[mm]	50.0
Inductance	[mH]	48.5
Magnet constant	[mT A^{-1}]	60.3
Operation parameters		
Operating temperature	[K]	77 (LN2)
Operating current	[A]	20
Ramp rate	[A s^{-1}]	0.05

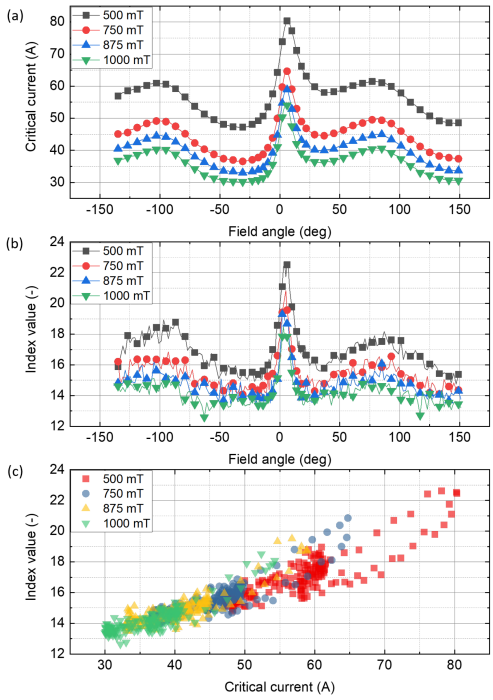

Fig. 1. Measurement results of field-dependent critical current $I_c(B,\theta)$ and index value $n(B,\theta)$, and the correlation between them.

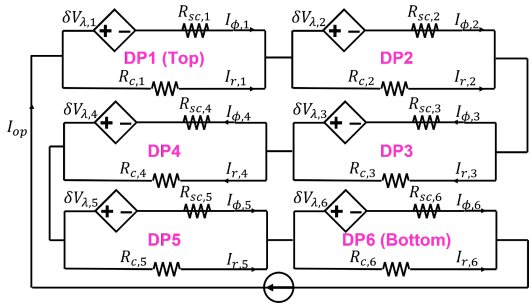

Fig. 2. Modified lumped-circuit model for module coil voltage simulation.

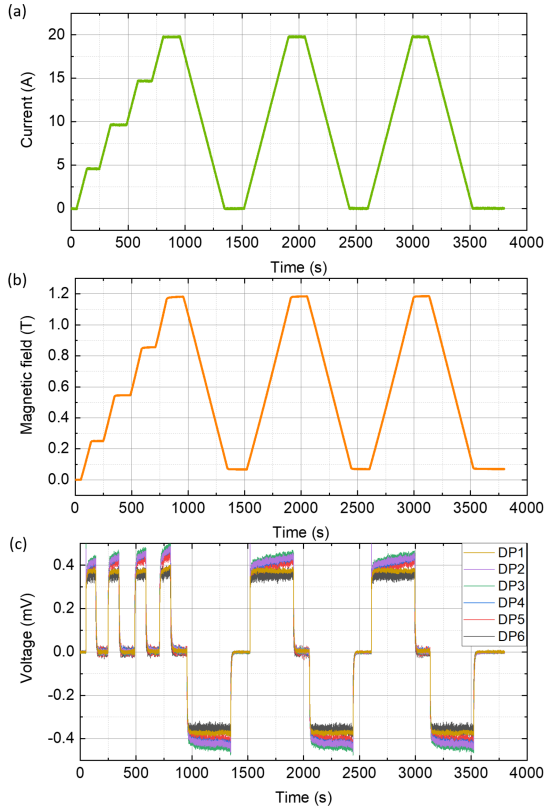

Fig. 3. Measurement results of (a) Operating current. (b) Coil central field. (c) Module coil voltages.

regardless of the field intensity B and angle θ. The result is described with:

$$n(B,\theta) \approx I_c(B,\theta) \times 0.2 + 7. \tag{1}$$

Therefore, the power-law $E-J$ model of Ohm's law for the screening current simulation is expressed with:

$$E = \left(\frac{E_c}{J_c(B,\theta)}\right)\left(\frac{|J|}{J_c(B,\theta)}\right)^{I_c(B,\theta)\times 0.2+7-1} J, \tag{2}$$

where E_c, J_c, E, and J indicate, respectively, critical electric field (usually 1 μ V/cm assumed), critical current density, electric field, and current density.

In this work, we adopt the finite element analysis using H-formulation for non-linear electromagnetic simulation to investigate screening current and compare simulated results with measured ones regarding coil voltages and the central magnetic field. Especially for the voltage comparison, a modified lumped circuit model provided in Fig. 2 is used. Each double pancake (DP) coil consisting of two single pancake coils is illustrated with one induced voltage source by flux linkage (δV_λ) and two resistances (superconductor and characteristic, R_{sc} and R_c). Here, $\delta V_{\lambda,i}$ is calculated with:

$$\delta V_{\lambda,i} = \frac{d}{dt}\lambda_{2i-1}\left(\equiv \sum_{j=1}^{N_{turn}^{2i-1}} \frac{\int\left[\int \boldsymbol{B}\cdot\boldsymbol{dS}_j\right] dw}{w_{2i-1}}\right) + \frac{d\lambda_{2i}}{dt}, \tag{3}$$

where i, λ_{2i-1}, N_{turn}^{2i-1}, and w_{2i-1} stand for, respectively, the index of DP, the average of total flux linkage of $2i-1^{\text{th}}$ SP, the number of turns, and conductor width. Note that we have discussed a deficiency of the conventional lumped circuit model using a constant inductance [25] through our previous work [26];

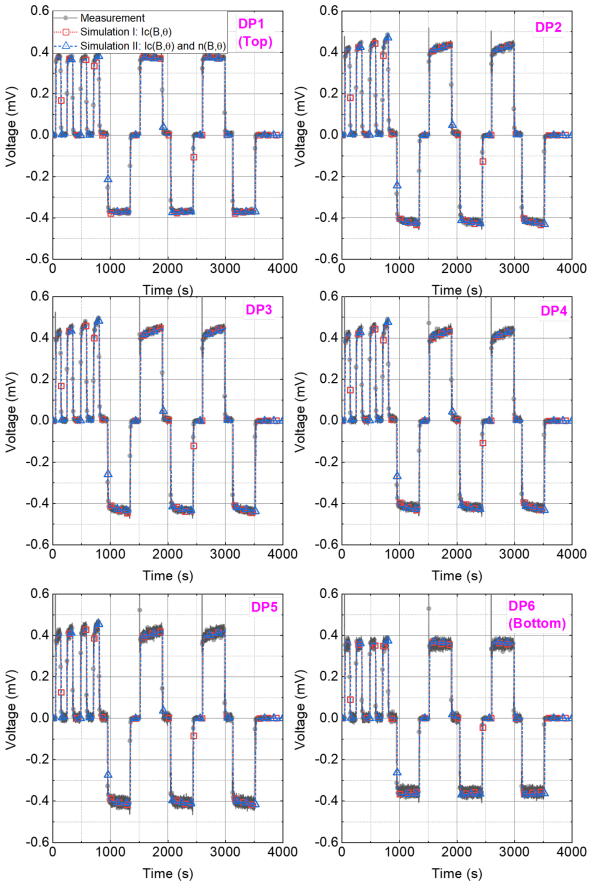

Fig. 4. Overview of comparison results of module coil voltages between simulation and measurement.

it investigated inductance variation by screening current [26], [27], [28], [29], thus proposing a modified model.

III. Result and Discussion

Fig. 3 presents measurement results of operating current, the coil central field, and module coil voltages. LBC4 was charged up to 20 A with a constant ramp rate of 0.05 A/s. The first charge consisted of four charge-hold steps to investigate the characteristics, e.g., outer joint resistance, inner joint resistance, and others. After this operation, an identical operation protocol was applied twice as a supplementary experiment for reproducibility confirmation. The peak magnetic field at the peak current is about 1.2 T, which is slightly smaller than the calculated value of 60.3 mT/A$^{-1}\times$ 20 A (probably due to screening current-induced field). Measured module coil voltages, except DP1 and DP6, present the inductive voltage increase from 0.4 mV to 0.5 mV. This agrees well with the expectation that inductance increases due to the flux penetration by screening current relaxation [26]. The deviation of DP1 and DP6 is discussed with comparison results.

Figs. 4–6 compare measurement and simulation results; Simulation I considers $I_c(B,\theta)$ and a constant n, while Simulation II considers both $I_c(B,\theta)$ and $n(B,\theta)$.

Fig. 4 confirms that Simulation I and II are able to reproduce most coil voltages, but Fig. 5 provides the difference between

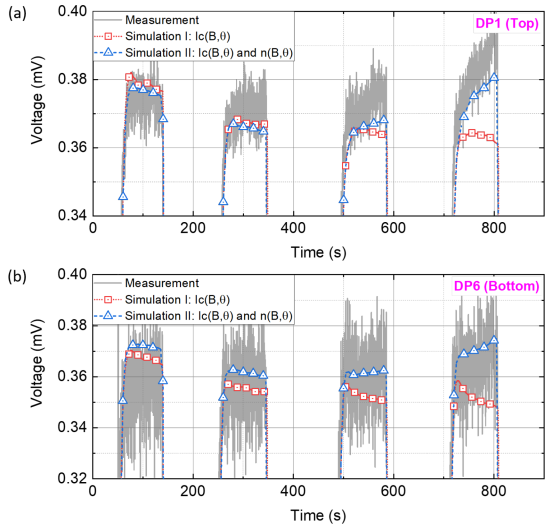

Fig. 5. Enlarged view of voltage comparison results of (a) top and (b) bottom coils. The blue line, the simulation result considering $I_c(B,\theta)$ and $n(B,\theta)$, traces the measured results, whereas notable discrepancy in the red line, the simulation result considering $I_c(B,\theta)$.

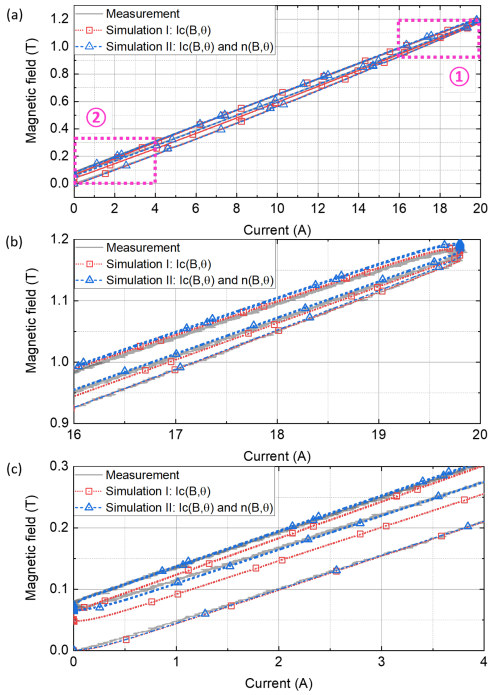

Fig. 6. Comparison of magnetic field between measurement and simulations. (a) Overview. (b)–(c) Enlarged view at the beginning of charge and discharge.

them. In DP1 and DP6, an unexpected voltage increase happens during the charge, which is not reproduced with Simulation I; meanwhile, we have confirmed little difference in simulation results (within a 5% error range) if an arbitrary constant n in a range of 20–40 is chosen. On the other hand, Simulation II reproduces this unexpected behavior well. This comparison clarifies that the proposed simulation approach considering $n(B,\theta)$ described in the previous section is practical for replicating measurement results, emphasizing a better agreement between Simulation II

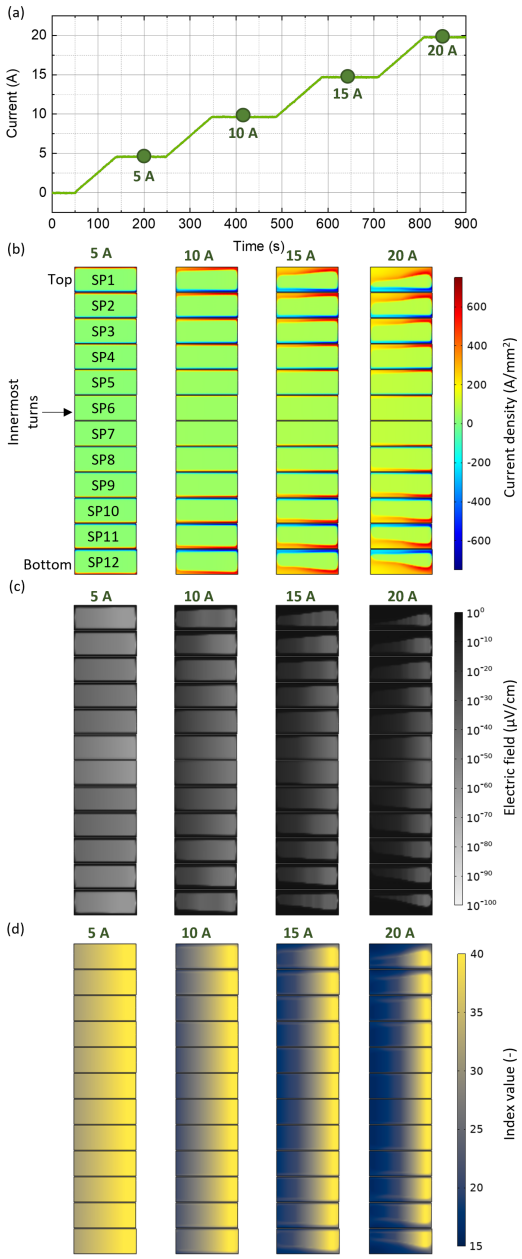

Fig. 7. Simulation results at the selected currents in (a) the beginning section of the first charge, (b) current density, (c) electric field, and (d) $n(B, \theta)$.

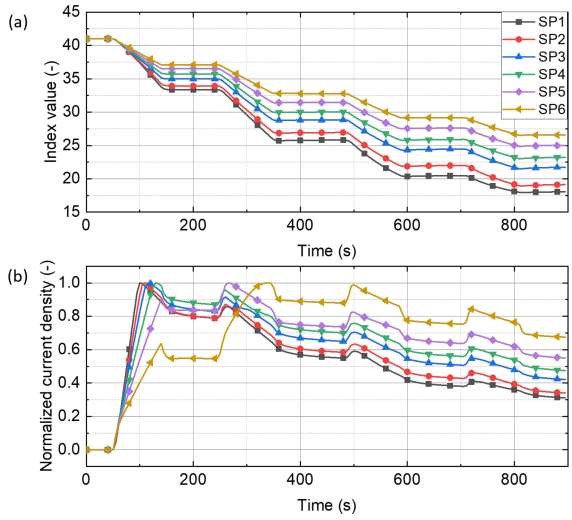

Fig. 8. Further current density analysis results to investigate the correlation between the n degradation and the screening current relaxation. (a) Field-dependent n behavior during the charge. (b) Peak-normalized current density change by screening current relaxation.

and measurement results. Fig. 6 supplements this argument in terms of magnetic field simulation. As shown in Fig. 6(a)–(b), Simulation I and II both seem to be practical in the magnetic field simulation. However, Fig. 6(c) shows the limit of using a constant n-value in simulating screening current if the coil current is low.

In conclusion, from this analysis, we confirm that n-value affects the amount of screening current induction and relaxation during the coil operation, as shown in Fig. 4 and Fig. 6. In addition, it is also confirmed that the remnant amount of screening current after the discharge is affected by n-value, as provided in Fig. 6(c). For further analysis of the effect of $n(B, \theta)$ on screening current, we have investigated current density, electric field, and n-value distributions in LBC4 at selected operating currents during the first charge in Fig. 3(a). Fig. 7 presents the investigation results.

This investigation explains that a low n-value is distributed at the edges of individual turns in each SP of LBC4, probably due to radial field concentration. Therefore, it concludes that a partially concentrated electric field induces a consequential voltage increase, as presented in Fig. 5. In addition, the conclusion obtained from further current density analysis is twofold. First, the screening current induction near the coil surfaces would be less than the simulation results using a constant n-value in 20–40. Second, its relaxation speed is faster than the simulated ones. To clarify the second argument, Fig. 8 summarizes the average value of n-value and peak-normalized current density at the selected top surfaces of SP1–6 in the upper half of LBC4 during the charge operation shown in Fig. 7(a). It indicates that the faster n degradation, the faster current density relaxation, and correspondingly, provides direct evidence for the second argument.

IV. Conclusion

This paper has reported the effect of field-dependent n-value on screening current and consequential NI REBCO coil behavior. The significance of this work is fourfold. First, the correlation between $I_c(B, \theta)$ and $n(B, \theta)$ has been formalized from the corresponding measurements with the linear regression, applied to the screening current simulation, and finally, evaluated for its necessity. Second, we have confirmed that the consideration of $n(B, \theta)$ can address some discrepancies between simulation and measurement in terms of coil voltages and the magnetic field hysteresis. Next, the electrical vulnerability near the top and bottom coil in a coil stack has been confirmed by simulation results that the electric field induction is concentrated near the top and bottom coils due to an intense radial field and consequential a low n-value. Last, a low n-value affects the screening current induction and its relaxation.

REFERENCES

[1] S. Kim, C. Lee, J. Bang, and S. Hahn, "Manipulation of screening currents in an (RE) $Ba_2Cu_3O_{7-x}$ superconducting magnet," *Mater. Res. Exp.*, vol. 6, no. 2, 2018, Art. no. 026004.

[2] J. Bang et al., "Field measurement and analysis of a 3 T 66 mm no-insulation HTS NMR magnet with screening current and manufacturing uncertainty considered," *IEEE Trans. Appl. Supercond.*, vol. 29, no. 5, Aug. 2019, Art. no. 4601305.

[3] Y. Li et al., "Screening-current-induced strain gradient on REBCO conductor: An experimental and analytical study with small coils wound with monofilament and striated multifilament REBCO tapes," *IEEE Trans. Appl. Supercond.*, vol. 30, no. 4, Jun. 2020, Art. no. 4702305.

[4] H. Ueda, Y. Awazu, K. Tokunaga, and S. Kim, "Numerical evaluation of the deformation of REBCO pancake coil, considering winding tension, thermal stress, and screening-current-induced stress," *Supercond. Sci. Technol.*, vol. 34, no. 2, 2021, Art. no. 024003.

[5] D. Kolb-Bond et al., "Screening current rotation effects: Scif and strain in REBCO magnets," *Supercond. Sci. Technol.*, vol. 34, no. 9, 2021, Art. no. 095004.

[6] Y. Yan, Y. Li, and T. Qu, "Screening current induced magnetic field and stress in ultra-high-field magnets using REBCO coated conductors," *Supercond. Sci. Technol.*, vol. 35, no. 1, 2021, Art. no. 014003.

[7] J. Bang et al., "A real-time monitoring system for investigating electromagnetic behaviors of an HTS coil," *IEEE Trans. Appl. Supercond.*, vol. 32, no. 6, Sep. 2022, Art. no. 9001505.

[8] S. Noguchi, T. Mato, and S. Hahn, "Inductive voltage of insert HTS coils due to coil deformation for ultra-high magnetic field generation," *IEEE Trans. Appl. Supercond.*, vol. 33, no. 5, Aug. 2023, Art. no. 4300905.

[9] G. Kim et al., "Investigation on nonuniform current density and shape deformation affecting magnetic field performance of a saddle-shaped no-insulation HTS cosine-theta dipole magnet," *Supercond. Sci. Technol.*, vol. 36, 2023, Art. no. 084002.

[10] J. Rhyner, "Magnetic properties and AC-losses of superconductors with power law current–voltage characteristics," *Physica C: Supercond.*, vol. 212, no. 3-4, pp. 292–300, 1993.

[11] R. Brambilla, F. Grilli, and L. Martini, "Development of an edge-element model for AC loss computation of high-temperature superconductors," *Supercond. Sci. Technol.*, vol. 20, no. 1, 2006, Art. no. 16.

[12] V. M. Zermeno, A. B. Abrahamsen, N. Mijatovic, B. B. Jensen, and M. P. Sørensen, "Calculation of alternating current losses in stacks and coils made of second generation high temperature superconducting tapes for large scale applications," *J. Appl. Phys.*, vol. 114, no. 17, 2013, Art. no. 173901.

[13] S. Mykola and G. Fedor, "A–V formulation for numerical modelling of superconductor magnetization in true 3D geometry," *Supercond. Sci. Technol.*, vol. 32, no. 11, 2019, Art. no. 115001.

[14] L. Bortot et al., "A coupled A–H formulation for magneto-thermal transients in high-temperature superconducting magnets," *IEEE Trans. Appl. Supercond.*, vol. 30, no. 5, Aug. 2020, Art. no. 4900911.

[15] S. Wang, H. Zhu, M. Wu, and W. Zhang, "Active disturbance rejection decoupling control for three-degree-of-freedom six-pole active magnetic bearing based on BP neural network," *IEEE Trans. Appl. Supercond.*, vol. 30, no. 4, Jun. 2020, Art. no. 3603505.

[16] D. K. Oh, "An alternative in H-formulation to the critical current model of HTS conductors," *IEEE Trans. Appl. Supercond.*, vol. 32, no. 7, Oct. 2022, Art. no. 4901808.

[17] C. Barth, G. Mondonico, and C. Senatore, "Electro-mechanical properties of REBCO coated conductors from various industrial manufacturers at 77 K, self-field and 4.2 K, 19 T," *Supercond. Sci. Technol.*, vol. 28, no. 4, 2015, Art. no. 045011.

[18] S. C. Wimbush and N. M. Strickland, "Utilising angle-dependent critical current data in the electromagnetic modelling of HTS coils," *Supercond. Sci. Technol.*, vol. 35, no. 2, 2022, Art. no. 024004.

[19] R. Taylor et al., "Transport current measurement of $I_c(T, B, \theta)$ and $n(T, B, \theta)$ for a bulk REBCO superconductor," *IEEE Trans. Appl. Supercond.*, vol. 33, no. 5, Aug. 2023, Art. no. 6800106.

[20] F. Liang et al., "Vortex shaking study of REBCO tape with consideration of anisotropic characteristics," *Supercond. Sci. Technol.*, vol. 30, no. 9, 2017, Art. no. 094006.

[21] Y. Liu et al., "Comparison of 2D simulation models to estimate the critical current of a coated superconducting coil," *Supercond. Sci. Technol.*, vol. 32, no. 1, 2018, Art. no. 014001.

[22] S. Hahn et al., "45.5-tesla direct-current magnetic field generated with a high-temperature superconducting magnet," *Nature*, vol. 570, no. 7762, pp. 496–499, 2019.

[23] X. Hu et al., "Analyses of the plastic deformation of coated conductors deconstructed from ultra-high field test coils," *Supercond. Sci. Technol.*, vol. 33, no. 9, 2020, Art. no. 095012.

[24] E. Berrospe-Juarez, F. Trillaud, V. M. Zermeño, and F. Grilli, "Advanced electromagnetic modeling of large-scale high-temperature superconductor systems based on H and TA formulations," *Supercond. Sci. Technol.*, vol. 34, no. 4, 2021, Art. no. 044002.

[25] S. Hahn, D. K. Park, J. Bascunan, and Y. Iwasa, "HTS pancake coils without turn-to-turn insulation," *IEEE Trans. Appl. Supercond.*, vol. 21, no. 3, pp. 1592–1595, Jun. 2011.

[26] J. Bang, J. Park, K. Choi, G. Kim, and S. Hahn, "A numerical method to calculate screening current-dependent self and mutual inductances of REBCO coils," *Supercond. Sci. Technol.*, vol. 36, 2023, Art. no. 085003.

[27] X. Deng et al., "An experimental and numerical study on the inductance variation of HTS magnets," *IEEE Trans. Appl. Supercond.*, vol. 25, no. 3, Jun. 2015, Art. no. 4603005.

[28] S. Chen et al., "Inductance of low-frequency small-scale high-temperature superconducting coils," *IEEE Trans. Appl. Supercond.*, vol. 29, no. 5, Aug. 2019, Art. no. 4901404.

[29] J. Lee and S. Noguchi, "A study on the critical current measurement of no-insulation HTS coils and the effect of screening current-induced voltage," *IEEE Trans. Appl. Supercond.*, vol. 33, no. 5, Aug. 2023, Art. no. 4602904.